Dielectric function and Van Hove singularities for In-rich $In_xGa_{1-x}N$ alloys: Comparison of N- and metal-face materials

P. Schley, R. Goldhahn,* A. T. Winzer, G. Gobsch, V. Cimalla, and O. Ambacher
Institute of Micro- and Nanotechnologies, Technical University Ilmenau, PF 100565, 98684 Ilmenau, Germany

H. Lu
Department of Physics, Nanjing University, Nanjing 210093, China

W. J. Schaff
Department of Electrical and Computer Engineering, Cornell University, Ithaca, New York 14853, USA

M. Kurouchi and Y. Nanishi
Department of Photonics, Faculty of Science and Engineering, Ritsumeikan University, 1-1-1 Noji-Higashi, Kusatsu, Shiga 525-8577, Japan

M. Rakel, C. Cobet, and N. Esser
ISAS-Institute for Analytical Sciences, Department Berlin-Adlershof, Albert-Einstein-Strasse 9, 12489 Berlin, Germany
(Received 26 September 2006; revised manuscript received 21 December 2006; published 14 May 2007)

Spectroscopic ellipsometry is applied in order to determine the complex dielectric function (DF) for In-rich $In_xGa_{1-x}N$ alloys with N-face polarity from near-infrared into the vacuum ultraviolet spectral region. The results are compared to corresponding data for metal-face films. The optical properties of both types of hexagonal films agree in the essential features which emphasizes that the extracted DFs do not depend on the polarity but represent therefore bulk characteristics. Besides the band gap, five critical points of the band structure are clearly resolved within the composition range of $1 \geqslant x \geqslant 0.67$. Their transition energies are determined by a fit of the third derivative of the DF. With increasing Ga content, all transitions undergo a continuous shift to higher energies characterized by small bowing parameters. Model calculations of the imaginary part of the DF close to the band gap that take the influence of band filling and conduction-band nonparabolicity into account are presented. A comparison to the experimental data yields the position of the Fermi energy. With the calculated values for the carrier-induced band-gap renormalization and the Burstein-Moss shift, the zero-density values for the fundamental band gaps are obtained. Their dependence on the alloy composition is described by a bowing parameter of $b=1.72$ eV.

DOI: 10.1103/PhysRevB.75.205204 PACS number(s): 78.20.Ci, 78.55.Cr, 78.66.Fd, 78.40.Fy

I. INTRODUCTION

The revision of the fundamental band gap for hexagonal InN from the long-accepted value of $E_0=1.89$ eV (Ref. 1) down to a value of about 0.7 eV (Refs. 2 and 3) has a strong impact on the whole $In_xGa_{1-x}N$ alloy system. McCluskey *et al.*[4] corrected the previously published bowing parameter from $b \sim 3.8$ eV to $b \sim 2.6$ eV assuming $E_0=0.8$ eV. Their absorption studies of Ga-rich layers covered an alloy composition range of $0 \leqslant x \leqslant 0.112$, and the band gaps were corrected for the pseudomorphic strain.

The first reports on a low band gap for InN initiated intensive work on growing high-quality In-rich alloys. A simplified analysis of absorption data for the composition range of $0.5 \leqslant x \leqslant 1.0$ yielded a much smaller bowing parameter of ~ 1.4 eV.[5] For those layers, grown on an AlN buffer layer, we reported recently[6] preliminary results on the determination of the complex dielectric function (DF) by applying spectroscopic ellipsometry (SE). Analyzing the imaginary part of the DF, a bowing parameter of 1.77 eV was determined for the band gap. In addition, five critical points (CPs) of the band structure, also known as Van Hove singularities, were identified in the high-energy part of the spectra that undergo a clear blueshift with increasing Ga content.

So far, almost all optical studies were carried out on In-face, i.e., metal-face (M-face), polar films. Several groups succeeded recently in growing nitrogen-face (N-face) InN films by plasma-assisted molecular beam epitaxy (PA-MBE).[7–9] The growth of N-face films can be carried out at higher temperatures compared to M-face material; this is probably going to be an advantage for the further improvement of the structural quality. *In situ* SE studies during growth revealed pseudo-DFs for N-face InN (Ref. 10) that match in the essential details to the previously published DF data for M-face layers.[11,12] Successful growth of corresponding high-quality N-face InGaN alloys with high In content has been demonstrated recently.[13,14] However, a determination of the DF for N-face films and a comprehensive analysis have not been carried out so far. In the ideal case, these results should coincide with the previous studies of M-face films because the DF represents a bulk property which should not depend on the polarity.

In this paper, we report on the determination of the dielectric function for N-face In-rich alloys by applying SE. The properties are compared to the results of metal-face films grown on different buffer layers. The experimentally ex-

TABLE I. Layer thickness, In content, and polarity as well as structural and electrical properties of the samples investigated.

Sample	AlN (nm)	GaN (nm)	LT-InN (nm)	InN (nm)	InGaN (nm)	x	Polarity	FWHM XRD Θ-2Θ($''$)	FWHM ω scan ω($'$)	n_e (10^{18} cm^{-3})	μ(300 K) (cm^2/V s)
M100	10	200		1070		1.00	M face	302	14	1.5	1200
M077	250				315	0.77	M face	350	27	2.5	260
M069	10	165			400	0.69	M face	320	16	2.0	140
M067	250				285	0.67	M face	331	28	3.4	150
N100			60	550		1.00	N face	176	24	6.5	780
N089			60	550	210	0.89	N face	407	26	7.0	190
N077			60	550	210	0.77	N face	720	35		

tracted DFs are compared to model calculations for degenerate nitride semiconductors. In extension of the previously published method,[15] the influence of inhomogeneous broadening on the determination of the transition energy at the Fermi wave vector is evaluated. Correcting these energies for the carrier-induced band-gap renormalization and Burstein-Moss shift, the zero-density band gaps are estimated and their bowing parameter is determined. The shift of the high-energy critical points is evaluated in the second part of the paper. The transition energies are obtained from a fit of the third derivatives of the DF.

II. EXPERIMENTAL DETAILS

In this work, the optical properties of four M-face and three N-face $In_xGa_{1-x}N$ alloy films will be compared. The nominally undoped single-crystal epitaxial layers were grown by PA-MBE on (0001) sapphire substrates. The layer thickness of the nucleation, buffer, and top layers as well as the composition and polarity are summarized in Table I. In order to obtain M-polarity films, growth was initiated by the deposition a 10 nm AlN nucleation layer, continued with a thick (165–250 nm) either GaN or AlN buffer layer, and finished by the deposition of the $In_xGa_{1-x}N$ film. The M-face InN film was deposited at a temperature of 470 °C, whereas the alloy films were grown at about 530 °C. Further details related to the epitaxial growth have been published elsewhere.[5]

The procedure to obtain the high-quality epitaxial N-face InGaN films can be summarized as follows.[7,13] Prior to growth, the (0001) sapphire substrate was thermally cleaned at 800 °C for 10 min in vacuum. Afterward, nitridation of the substrate surface was carried out at 550 °C for 1 h. At first, a ~60-nm-thick low-temperature (LT) InN buffer layer was deposited at 300 °C. Then, the temperature was raised to 530 °C and thereafter a ~550-nm-thick InN film was grown on the LT-InN buffer. For two samples, 210-nm-thick In-rich alloy films were grown at 550 °C on top. Investigations of these samples by coaxial impact-collision ion scattering spectroscopy, convergent beam electron-diffraction method, as well as chemical etching revealed that the films have N-face polarity.[16]

The structural properties of $In_xGa_{1-x}N$ layers were characterized by x-ray diffraction (XRD) including Θ-2Θ scans, ω scans, and high-resolution reciprocal space maps of the symmetric (0002) as well as asymmetric (20$\bar{2}$5) reflexes. The corresponding full widths at half maximum (FWHM) of the (0002) reflexes are given in Table I. The XRD analysis shows that high-quality wurtzite-structured InGaN epitaxial layers were formed with their c axis perpendicular to the substrate surface. The lattice constants for the In-(M100) and N-face (N100) InN layers amount to c=5.704 Å (a=3.537 Å) and c=5.703 Å (a=3.535 Å), respectively, with an accuracy of ±0.002 Å. They are very close to the recently published values for strain-free InN of c=5.699±0.004 Å and a=3.535±0.005 Å.[17] The In atomic fraction of the ternary alloys were independently determined from the c as well as from the a lattice constants via Vegards law. The values differ by less than 0.02; the average of both compositions is given in Table I. It emphasizes that the films are nearly strain-free.

Because of the different layer thicknesses, we do not observe a correlation of the growth conditions to the structural properties. However, room-temperature Hall measurements revealed for the N-face InN a higher electron concentration n_e and a lower mobility μ compared to the M-face sample (see Table I).

The optical properties of all samples were investigated by SE. The ellipsometric parameters Ψ and Δ were measured by a commercially available ellipsometer at multiple angles of incidence (Φ=62°, 68°, and 74°) and at photon energies of up to 5 eV. For the investigations in the UV-VUV spectral region from 4 to 9.5 eV, we used the ellipsometer attached to the Berlin electron storage ring (BESSY II). These data refer to Φ=67.5°. The room-temperature photoluminescence (PL) was excited by the 514.5 nm line of an Ar^+-ion laser, then dispersed by a 2 m monochromator, and detected by a liquid-nitrogen-cooled Ge photodiode or InGaAs photodiode. All spectra are corrected for the spectral response of the system.

III. RESULTS AND DISCUSSION

The real (ε_1) and the imaginary part (ε_2) of the complex DF ($\bar{\varepsilon}=\varepsilon_1+i\varepsilon_2$) were obtained by fitting the experimental data Ψ and Δ using a multilayer model similar to the procedure reported in Ref. 18. Atomic force microscopy revealed a smooth film morphology with a root-mean-square roughness below 1.5 nm for the binary layers and below 2.9 nm for the

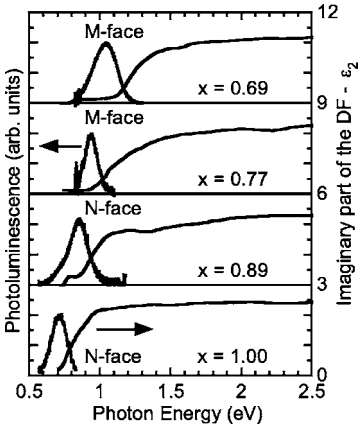

FIG. 1. PL spectra and imaginary parts of the DF for M- and N-face $In_xGa_{1-x}N$ alloys at room temperature. The ε_2 data have been vertically shifted and PL curves have been normalized to equal amplitude for the sake of clarity.

alloys. For the interpretation of ellipsometry data, the roughness of the surface was treated in Bruggeman effective-medium approximation assuming 50% of voids in a matrix of InGaN. In this work, ε_1 and ε_2 were independently fitted at every photon energy, i.e., without making any assumption concerning the spectral dependence of $\bar{\varepsilon}$. The Kramers-Kronig consistency of the optical data was proven by numerical integration of ε_2. Our approach is different from the work of Kasic *et al.* that used a critical-point model dielectric function (MDF) in order to determine the DF for InN layers.[11] Note that the MDF assumes an empty parabolic conduction band that is not the case for InN due to the high electron concentration and the nonparabolicity arising from the low band gap.[19] For films with (0001) orientation, i.e., with c axis normal to the surface, the extracted data are very close to the ordinary DF that was recently demonstrated by a comparison of a-plane and c-plane InN films.[12,20] Only small deviations in the magnitude are detected for photon energies above 8 eV, attributed to the large angle of refraction in this range.

A. Experimental data around the band gap

Figure 1 shows representative examples of the imaginary part of the DF (ε_2) around the band gap for M- and N-face InGaN films as well as the emission spectra taken at room temperature. Corresponding spectra for the M-face $In_{0.67}Ga_{33}N$ can be found elsewhere.[6] The shape of ε_2 for the N-face InN film around the gap is very similar to the previously published results[15] for the M-face layer. The imaginary part of the DF becomes constant above 1 eV. The emission maximum is found at 0.71 eV.

For the alloys, both the onset of ε_2 and the PL peak undergo a clear shift to higher energies with increasing Ga content. The InGaN films grown on GaN buffer (x=0.69) and on LT-InN buffer (x=0.89) exhibit a much sharper increase of ε_2 compared to the film (x=0.77) grown directly on AlN, which shows the impact of the buffer layers. Both GaN and LT-InN buffer layers lead to improved structural properties of the alloy films as indicated by the x-ray data summarized in Table I. For example, comparing the films with nearly identical In content, the FWHM of the ω scans amounts to 16 (28) arc min for M069 (M067), i.e., the film grown on GaN buffer exhibits a much narrower linewidth. For comparison, the InN film (M100) on GaN buffer is characterized by 14 arc min.

Nearly all reports on the determination of the band gap of InN and related alloys evaluate the spectral dependence of the absorption coefficient (α) determined by transmission measurements most of the times. The analysis is based on the fact that α is proportional to the imaginary part of the DF via the relation $\alpha=\omega\varepsilon_2/(nc_0)$ (ω, angular frequency of light; c_0, vacuum speed of light). The spectral dependence of the refractive index n is neglected as criticized in the report by Butcher and Tansley.[21] Then, a square-root dependence of ε_2 (and thus α) on the photon energy $\hbar\omega$ is assumed as valid for a three-dimensional M_0 critical point with parabolic band structure and an empty conduction band. Finally, the absorption edge (or band gap) is estimated by extrapolating the experimental data to zero. To improve the determination of the band gap, it is necessary to analyze directly ε_2 as was briefly demonstrated in our recent paper for M-face InN and InAlN layers.[15]

B. Influence of high carrier densities on the DF

In the following, the method for analyzing ε_2 will be discussed in details by means of two examples: the N-face alloy with x=0.89 and the M-face material with x=0.69. The analysis starts from a calculation of the imaginary part of the DF that is proportional to the joint density of states via

$$\varepsilon_2(\hbar\omega) \sim \frac{1}{(\hbar\omega)^2}\frac{2}{(2\pi)^3}\int_{BZ}|P_{cv}|^2[1-f(E_c)] \times \delta(E_c - E_v - \hbar\omega)d^3k, \quad (1)$$

where P_{cv} is the momentum matrix element. The Fermi distribution function for the conduction-band (CB) electrons is denoted by $f(E_c)$, i.e., the term $[1\text{-}f(E_c)]$ takes into account the fact that the absorption requires empty states in the CB. E_c and E_v are the CB and valence-band (VB) energy, respectively. The integration is carried out in the reciprocal (k) space over the whole Brillouin zone (BZ).

Carrier-induced band-gap renormalization (BGR) Δ_{BGR} leads to a shrinkage of the intrinsic band gap E_0 due to electron-electron interaction and electron-ionized impurity interaction.[19] The CB shift resulting from the electron-electron interaction is given by

$$\Delta E_{e\text{-}e} = -\frac{2e^2k_F}{4\pi^2\varepsilon_0\varepsilon_r} - \frac{e^2k_{TF}}{8\pi\varepsilon_0\varepsilon_r}\left[1 - \frac{4}{\pi}\arctan\left(\frac{k_F}{k_{TF}}\right)\right], \quad (2)$$

where $k_F=(3\pi^2n_e)^{1/3}$ is the Fermi wave vector, $k_{TF}=(2/\sqrt{\pi})\times(k_F/a_B)^{1/2}$ denotes the Thomas-Fermi screening wave vector, ε_r represents the static dielectric constant, and $a_B=0.53\times10^{-10}\varepsilon_r m_0/m_e^*$ is the effective Bohr radius [m_e^*, density-of-states effective electron mass as defined below by Eq. (5)]. An ε_r value of 9.5 was proposed[22] for hexagonal InN with a

band gap of 0.67 eV. It is also used as approximation for alloys with $x>0.67$. For comparison, $\varepsilon_r=10.4$ was reported[23] for GaN with a much higher gap of $E_0=3.447$ eV. The contribution of the electron-ion interaction to the CB shift can be written as

$$\Delta E_{e\text{-}i} = -\frac{4\pi e^2 n_e}{4\pi\varepsilon_0\varepsilon_r a_B k_{\mathrm{TF}}^3}. \tag{3}$$

For example, BGR ($\Delta_{\mathrm{BGR}}=\Delta E_{e\text{-}e}+\Delta E_{e\text{-}i}$) amounts to −65 and −105 meV for carrier concentrations of 2.0×10^{18} cm^{-3} (sample M069) and 7.0×10^{18} cm^{-3} (sample N089), respectively.

For the ε_2 calculations via Eq. (1), the curvature of the VB and CB is needed in addition. The VB can be described by a parabolic approximation with an effective mass for the holes of $m_h=0.5m_0$.[24] Since the CB of InN and the In-rich alloys is highly nonparabolic (due to the low band-gap value), we applied the formula given by Kane's two-band $\mathbf{k}\cdot\mathbf{p}$ model[25] as in previous studies,[19]

$$E_c(k) = \frac{E_{\mathrm{BGR}}}{2} + \frac{\hbar^2k^2}{2m_0} + \frac{1}{2}\sqrt{E_{\mathrm{BGR}}^2 + 4E_P\frac{\hbar^2k^2}{2m_0}}, \tag{4}$$

where $E_{\mathrm{BGR}}=E_0+\Delta_{\mathrm{BGR}}$ is the renormalized band-gap energy. Note that E_{BGR} instead of E_0 has to be inserted into Eq. (4) in order to account for the enhanced band interaction. E_P is an energy parameter related to the momentum matrix element P_{cv}. A linear dependence on the alloy composition is assumed between the values for InN and GaN of 10 eV (Ref. 19) and 13.2 eV,[26] respectively. The density-of-states effective electron mass becomes k dependent and is calculated from Eq. (4) via

$$m_e^*(k) = \frac{\hbar^2 k}{dE_c(k)/dk}. \tag{5}$$

Finally, the energetic position of the Fermi level above the conduction-band minimum $[\Delta E_c(k_F)]$ at the Fermi wave vector k_F is needed. It follows from the calculation of the electron density via

$$n_e = \int_{E_{\mathrm{BGR}}}^{+\infty} f(E_{\mathrm{C}})g(E)dE. \tag{6}$$

The density of states $g(E)$ is obtained from Eq. (4). E_F is adjusted in order to achieve matching with the experimental electron concentrations of Table I. Thereby, the Fermi energy is determined to be 59 and 165 meV above the CB at $k=0$ for samples M069 and N089, respectively. The energy of the VB at k_F is 11 and 26 meV lower in comparison to the Γ point [this quantity is denoted by $\Delta E_v(k_F)$]. This means that a small amount of the Burstein-Moss shift $\Delta E_{\mathrm{cv}}(k_F)=\Delta E_c(k_F)+\Delta E_v(k_F)$ is caused by the curvature of the VB.

Taking into account Δ_{BGR} and disregarding additional broadening effects in the first step of the calculation, one obtains a shape for ε_2 plotted by dashed lines in Figs. 2(a) and 2(b) for the N-face $In_{0.89}Ga_{0.11}N$ film and the M-face $In_{0.69}Ga_{0.31}N$ film, respectively. The VB-CB splitting at the Fermi wave vector (Fermi energy E_F) is given for comparison (vertical lines). Good agreement to the extracted experimental data (solid lines in Fig. 2) is achieved already. Note that neither the band gap nor the position of E_F corresponds to the rise of ε_2 from zero that emphasizes the limitations of the extrapolation method.

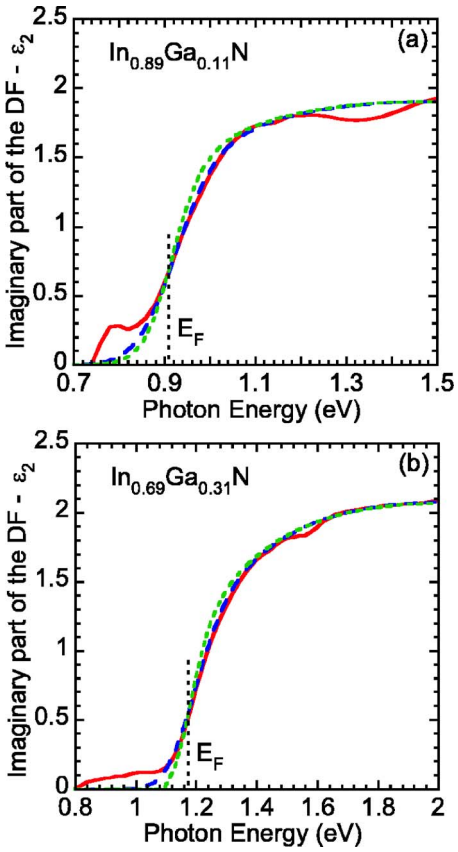

FIG. 2. (Color online) Calculated shape of the imaginary part of the DF without (dashed lines) and with (long-dashed lines) broadening effects in comparison to the experimental data (solid lines) for the N-face $In_{0.89}Ga_{0.11}N$ (a) and the M-face $In_{0.69}Ga_{0.31}N$ films (b). Band filling and band-gap renormalization are taken into account for calculations as explained in the text.

In the final step, the influence of inhomogeneous line shape broadening should be considered. In order to account for these effects, the calculated ε_2 curves were convoluted with a Gaussian function

$$\varepsilon_{2,b}(\hbar\omega) = \frac{1}{\Delta\sqrt{\pi}}\int_{-\infty}^{\infty}\varepsilon_2(E')\exp\left[-\left(\frac{E'-\hbar\omega}{\Delta}\right)^2\right]dE', \tag{7}$$

where Δ denotes the Gaussian broadening parameter. With Δ values of 60 and 80 meV, we obtain the results for the two samples that are plotted in Figs. 2(a) and 2(b), respectively, by long-dashed lines. Figure 2 demonstrates that inhomogeneous broadening has a negligible influence on an accurate determination of the intrinsic band gap, i.e., all curves lie upon each other at the Fermi energy. As a consequence, ε_2 values of 0.85 (N089) and 0.5 (M069) corresponding to the optical transitions at k_F for that the splitting between VB and CB $[E_F(k_F)]$ amount to 0.91 and 1.17 eV, respectively. Using the calculated values for Δ_{BGR} and $\Delta E_{\mathrm{cv}}(k_F)$, we attain the zero-density band gaps for the two samples. The correction

TABLE II. PL peak energy and Fermi energy as well as contributions to band-gap renormalization and Burstein-Moss shift used for determining the intrinsic band gaps E_0 (accuracy ±0.02 eV).

Sample	PL peak (eV)	$E_F(k_F)$ (eV)	$\Delta E_{e\text{-}e}$ (meV)	$\Delta E_{e\text{-}i}$ (meV)	Δ_{BGR} (meV)	$\Delta E_c(k_F)$ (meV)	$\Delta E_v(k_F)$ (meV)	$\Delta E_{cv}(k_F)$ (meV)	E_0 (eV)
M100		0.69	−29	−28	−57	62	8	70	0.68
M077	0.94	1.05	−36	−30	−66	65	11	76	1.04
M069	1.05	1.17	−36	−29	−65	59	11	70	1.16
M067	1.08	1.27	−40	−32	−72	72	15	87	1.25
N100	0.71	0.78	−59	−47	−106	176	24	200	0.69
N089	0.84	0.91	−57	−48	−105	165	26	191	0.82

yields values of 0.82 eV (N089) and 1.16 eV (M069). The method for determining zero-density band gaps is corroborated by scanning tunneling spectroscopy studies of the M-face sample.[27] Veal *et al.* obtained an experimental VB-CB splitting of 1.1±0.1 eV. Taking into account the Δ_{BGR} shift of −60 meV, it corresponds to a gap of 1.16±0.1 eV, in excellent agreement with our findings.

The experimentally determined ε_2 in Figs. 2(a) and 2(b) shows a deviation from the calculated results in the range between 1.3 and 1.4 eV (sample N089) and at 1.5 eV (sample M069), respectively. This effect is attributed to the influence of the surface accumulated electrons.[27,28] The size of the deviation depends on the relative position of the band edges with respect to the Fermi stabilization energy (E_{FS}). E_{FS} can be described as the average energy level of native defects. In $In_xGa_{1-x}N$ with $x>0.34$, the conduction-band edge (CBE) is below E_{FS}.[29] Thus, the native defects are mainly donorlike and raise the electron concentration along with E_F. With increasing Ga content, the CBE shifts to E_{FS}. It results in a decreasing influence of the surface accumulation layer to the optical measurements. So, the deviation in ε_2 is smaller for $In_{0.69}Ga_{0.31}N$ than for $In_{0.89}Ga_{0.11}N$. Finally, the onset of absorption (solid lines in Fig. 2) below 0.9 eV (a) and 1.1 eV (b) is attributed to interface formation between the buffer layer and InGaN films. The effect is more pronounced for the N-face sample with the highest Ga content (N077) that is therefore disregarded for the following discussion of the band-gap shift.

C. Bowing parameter of the band gap

Table II provides a summary of the relevant parameters for determining the intrinsic band gaps from the experimentally obtained $E_F(k_F)$ data for all studied samples. The final values for E_0 (accuracy ±0.02 eV) as function of alloy composition are displayed in Fig. 3. For comparison, strain-corrected band gaps of Ga-rich InGaN alloys reported by McCluskey *et al.*[4] and Pereira *et al.*[30] are provided in addition. In both studies, the E_0 values were obtained from the analysis of absorption studies, but different criteria were used to define the band gap. The photoreflectance measurements[31] for the range $0 \leqslant x \leqslant 0.20$ provided probably the most accurate results for Ga-rich alloys. However, only the compositional dependence was reported but not the quantitative gap values. These data are therefore not added to Fig. 3. Note that the dependence of Ref. 31 reproduces well the results of Ref. 4.

Taking into account the additional data points for intrinsic band gaps, the bowing parameter b for the InGaN material system can be reevaluated. The transition energy E_{CP} of any critical point of the band-structure gap as a function of composition is represented by

$$E_{CP}(x) = xE_{CP,InN} + (1-x)E_{CP,GaN} - bx(1-x). \quad (8)$$

As already discussed in Sec. I, the bowing parameter depends very sensitively on the values chosen for the two binary compounds. The splitting between the Γ_9^v valence band and the Γ_7^c conduction band represents the fundamental band gaps of both InN and GaN. Reflectance and PL studies of a strain-free homoepitaxial GaN layer[32] yielded at room temperature a free excitonic transition energy of 3.422 eV, from that, with a binding energy of 25 meV, $E_{cp,GaN}=E_{0,GaN}=3.447$ eV follows. Although the carrier concentrations dif-

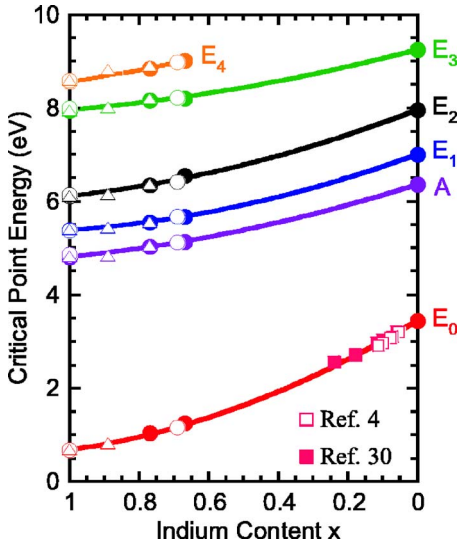

FIG. 3. (Color online) Band gap and critical-point energies of InGaN alloys as a function of the indium content. Open circles and triangles refer to the samples on GaN buffer and LT-InN buffer, respectively. Full circles are attached to samples on AlN buffer. Open and filled squares display measured band-gap values adapted from Refs. 4 and 30. The solid lines represent the best fits for determining the bowing parameters.

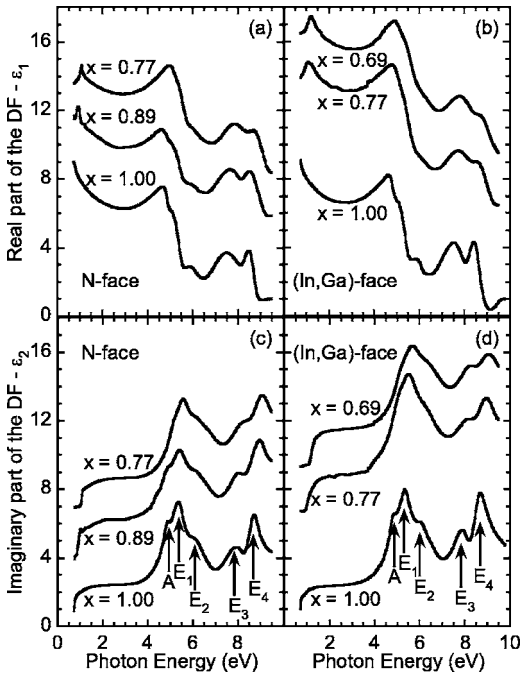

FIG. 4. Real [(a) and (b)] and imaginary parts [(c) and (d)] of the DF for N-face (left) and M-face (right) $In_xGa_{1-x}N$ obtained from fitting ellipsometric data Ψ and Δ. The alloy data are vertically shifted for the sake of clarity according to the indium content.

fer appreciably for the InN samples studied here, the values determined for intrinsic band gaps are very close. They amount to 0.68 eV (M100) and 0.69 eV (N100). The small difference emphasizes the reliability of the method for determining band gaps from the imaginary part of the DF. A fit of absorption data[29] for a low-carrier-density sample yielded also 0.68 eV, whereas from the MDF analysis of SE data a value of 0.65 eV was extrapolated.[11] Applying the analysis as described above to the ordinary and extraordinary dielectric tensor components of an $(11\bar{2}0)$ *a*-plane InN film with $n_e=6\times10^{18}$ cm^{-3}, one obtains 0.69 eV.

The largest uncertainty of the intrinsic band-gap values is probably caused by the Δ_{BGR} and $\Delta E_c(k_F)$ corrections. Therefore, we propose the use of $E_0=0.68$ eV for the intrinsic gap of wurtzite InN. Then, a fit of the current data together with the results from Ref. 4 yields a bowing parameter of $b=1.72$ eV. The fit is shown by the full line in Fig. 3. It differs only slightly from our previous studies,[6] where $b=1.77$ eV was obtained (only based on M-face In-rich alloys). For comparison, $b=1.51$ eV is fitted with the gaps for Ga-rich materials from Ref. 30 and the In-rich data of the present work. Some theoretical results should be mentioned as well. First-principles calculations yielded bowing parameters of 1.7 eV (Ref. 33) and 1.44 eV.[34]

D. High-energy critical points of the band structure

Figure 4 provides the real and imaginary parts of the DFs for the N-face (a) and M-face (b) InGaN alloys in comparison to the data of InN over the whole investigated range of photon energies. Because of *c*-axis orientation normal to the surface, the DFs are very close to the ordinary tensor component.[12,20] First of all, the excellent agreement of the N-face InN data with the M-face ones should be noticed. It provides a further proof that N-polar material can be grown with high optical quality. Besides the gap structure, the shape of the ordinary tensor component is strongly influenced by contributions arising from at least five critical points of the band structure in the energy range above 4.5 eV. The spectral dependence of the imaginary part is consistent with the results of *ab initio* calculations of the ordinary optical properties of hexagonal InN.[35] In order to achieve these results, electron-hole interaction was taken into account over the whole energy range. The excitonic effects cause an overall redshift of the entire spectra and a redistribution of oscillator strength with respect to the single-particle band structure and DF. Ellipsometric studies[11,36,37] carried out up to 6.5 eV yielded nearly identical results as presented here.

All Van Hove singularities are as well clearly resolved for the alloys despite a larger broadening, which confirms the good crystalline quality of the InGaN films. As expected for an alloy system, they undergo a continuous shift to higher energies with increasing Ga content.

For a further evaluation of the compositional dependence of the CP energies, it is necessary to pay special attention to the values for the binary compounds again. Until now, transition energies of CPs for InN were estimated either from digitizing peaks and shoulders of the ε_2 spectra[12,20,36,37] or by applying the MDF line shape.[11] Recently, we presented a more accurate approach to evaluate the Van Hove singularities by calculating the third derivative of the point-by-point DF (after surface roughness correction) multiplied by the square of the photon energy E.[6,15] The resulting spectra can be fitted[38] via

$$\frac{d^3}{dE^3}(E^2\bar{\varepsilon}) = \sum_{j=1}^{5} e^{i\cdot\phi_j}\frac{C_j}{(E+i\Gamma_j-E_{\mathrm{CP},j})^{n/2}}, \tag{9}$$

where ϕ_j, C_j, Γ_j, and $E_{\mathrm{CP},j}$ denote the phase angle, the magnitude, the broadening energy, and the transition energy of the *j*th CP, respectively. Both the real and imaginary parts are fitted in order to increase the reliability of the results. The transitions A-E_3 of all samples are well represented by $n=6$, whereas $n=7$ yields the best results for E_4. It corresponds to four two-dimensional and one one-dimensional critical points, respectively.

A comparison of the current data for hexagonal InN with the results from Refs. 11 and 36 is given in Table III. The third derivative analysis with its higher accuracy yields a slightly lower value especially for the *A* transition. This is not surprising because it appears only as a low-energy shoulder of E_1 as can be seen in Fig. 4. Digitizing the shoulder leads to an overestimation of the transition energy. In the following, we use the data of the M-face sample (M100) for the determination of the bowing parameter.

Prior to this, examples of the data analysis for the alloys are given. Applying Eq. (9) to the data of the N-face $In_{0.89}Ga_{0.11}N$ layer and the M-face $In_{0.69}Ga_{0.31}N$ layer, one obtains the curves shown in Figs. 5(a) and 5(b). Both parts of the DF are nicely reproduced. The InGaN films with identi-

TABLE III. Comparison of transition energies at Van Hove singularities for InN at room temperature.

Sample	A (eV)	E_1 (eV)	E_2 (eV)	E_3 (eV)	E_4 (eV)
M100	4.81	5.38	6.12	7.95	8.57
N100	4.82	5.39	6.12	7.95	8.60
InN[a]	4.84	5.41	6.10		
InN[b]	4.85	5.38	6.18		

[a]Reference 11.
[b]Reference 36.

cal In content but different polarities (M077, N077) show good agreement of critical-point energies within 20 meV. These results as well as the data for the other alloys are plotted in Fig. 3. The small scattering of the data allows one to determine the bowing parameters for the CPs. The third derivative analysis of the DF yielded for GaN (Ref. 39) the following transition energies: 6.36 eV (A), 7.00 eV (E_1), 7.96 eV (E_2), and 9.25 eV (E_3). The E_4 CP lies above the currently investigated spectral range and is therefore not included here. The compositional dependence of the transition energies, as indicated in Fig. 3 by the solid lines, is described by bowing parameters of b=0.80 eV (A), 1.07 eV (E_1), 1.03 eV (E_2), and 0.66 eV (E_3). The bowing parameters of highly energetic CPs are considerably lower than for the band gap. As has been demonstrated recently,[15] this is also the case for InAlN alloys. The bowing parameters of CPs are essential for parametrized models of the DF.[40]

IV. SUMMARY

In summary, we have determined the dielectric function of In-rich metal- and nitrogen-face InGaN alloys from the near-infrared into the vacuum ultraviolet spectral region. Films grown on GaN or LT-InN buffer layers show a much sharper absorption edge (imaginary part of the DF ε_2) compared to layers grown on AlN. This is interpreted as a consequence of an improved structural quality. Furthermore, we have calculated the spectral shape of ε_2 in the vicinity of the band gap including the band-filling effects (ΔE_F, Δ_{BGR}) and the nonparabolicity of the conduction band. By analyzing the experimental data with theoretical results, the zero-density band gaps are obtained. From that, the bowing parameter is extracted. The InGaN band gap is characterized by a b of 1.72 eV. Applying a third derivative based DF line shape fitting procedure yields the transition energies in the range of the highly energetic critical points of the band structure. From the transition energies, the bowing parameters for the compositional dependence of four critical points are derived. It was demonstrated that the results (e.g., dielectric functions, transition energies) do not depend on the polarity and therefore growth conditions. Thus, all extracted quantities represent bulk properties of In-rich InGaN alloys.

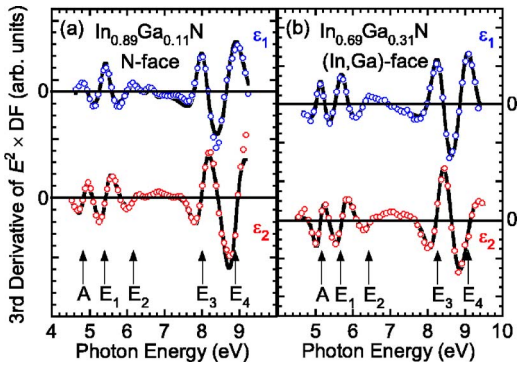

FIG. 5. (Color online) Fit of the third derivative of the DF for the N-face $In_{0.89}Ga_{0.11}N$ sample (a) and the metal-face $In_{0.69}Ga_{0.31}N$ sample (b). The circles represent the experimental data and the solid lines are the best fits.

ACKNOWLEDGMENTS

P.S. and R.G. acknowledge financial support by Thüringer Ministerium für Wirtschaft, Technologie und Arbeit (B509-04011) and by Deutsche Forschungsgemeinschaft (GO 1378/3), respectively. The ellipsometric studies at BESSY were supported by the BMBF (Grants Nos. 05KS4KTB/3 and 05ES3XBA/5). M.R., C.C., and N.E., are supported by the SFB290 of the Deutsche Forschungsgemeinschaft (DFG), the Bundesministerium für Bildung und Forschung and the Senatsverwaltung für Wissenschaft, Forschung und Kultur des Landes Berlin. W.J.S. acknowledges support from ONR Contract No. N000149910936.

*Electronic address: ruediger.goldhahn@tu-ilmenau.de

[1] T. Tansley and C. Foley, J. Appl. Phys. **59**, 3241 (1986).
[2] V. Davydov, A. Klochikhin, R. Seisyan, V. Emtsev, S. Ivanov, F. Bechstedt, J. Furthmüller, H. Harima, V. Mudryi, J. Aderhold, O. Semchinova, and J. Graul, Phys. Status Solidi B **229**, R1 (2002).
[3] J. Wu, W. Walukiewicz, K. M. Yu, J. W. Ager III, E. E. Haller, H. Lu, W. J. Schaff, Y. Saito, and Y. Nanishi, Appl. Phys. Lett. **80**, 3967 (2002).
[4] M. McCluskey, C. Van de Walle, L. Romano, B. Krusor, and N. Johnson, J. Appl. Phys. **93**, 4340 (2003).
[5] J. Wu, W. Walukiewicz, K. M. Yu, J. W. Ager III, E. E. Haller, H. Lu, and W. J. Schaff, Appl. Phys. Lett. **80**, 4741 (2002).
[6] P. Schley, R. Goldhahn, A. T. Winzer, G. Gobsch, V. Cimalla, O. Ambacher, M. Rakel, C. Cobet, N. Esser, H. Lu, and W. J. Schaff, Phys. Status Solidi B **243**, 1572 (2006).
[7] Y. Nanishi, Y. Saito, and T. Yamaguchi, Jpn. J. Appl. Phys., Part 1 **42**, 2549 (2003).
[8] X. Wang, S.-B. Che, Y. Ishitani, and A. Yoshikawa, J. Appl. Phys. **99**, 073512 (2006).
[9] G. Koblmüller, C. S. Gallinat, S. Bernardis, J. S. Speck, G. D. Chern, E. D. Readinger, H. Shen, and M. Wraback, Appl. Phys.

Lett. **89**, 071902 (2006).
[10] M. Yoshitani, K. Akasaka, X. Wang, S.-B. Che, Y. Ishitani, and A. Yoshikawa, J. Appl. Phys. **99**, 044913 (2006).
[11] A. Kasic, E. Valcheva, B. Monemar, H. Lu, and W. J. Schaff, Phys. Rev. B **70**, 115217 (2004).
[12] R. Goldhahn, P. Schley, A. T. Winzer, M. Rakel, C. Cobet, N. Esser, H. Lu, and W. J. Schaff, J. Cryst. Growth **288**, 273 (2006).
[13] M. Kurouchi, T. Yamaguchi, H. Naoi, A. Suzuki, T. Araki, and Y. Nanishi, J. Cryst. Growth **275**, e1053 (2005).
[14] H. Naoi, M. Kurouchi, D. Muto, S. Takado, T. Araki, T. Miyajima, H. Na, and Y. Nanishi, Phys. Status Solidi A **203**, 93 (2006).
[15] R. Goldhahn, P. Schley, A. T. Winzer, G. Gobsch, V. Cimalla, O. Ambacher, M. Rakel, C. Cobet, N. Esser, H. Lu, and W. J. Schaff, Phys. Status Solidi A **203**, 42 (2006).
[16] Y. Nanishi, Y. Saito, T. Yamaguchi, M. Hori, F. Matsuda, T. Araki, A. Suzuki, and T. Miyajima, Phys. Status Solidi A **200**, 202 (2003).
[17] E. Dimakis, E. Iliopoulos, K. Tsagaraki, A. Adikimenakis, and A. Georgakilas, Appl. Phys. Lett. **88**, 191918 (2006).
[18] R. Goldhahn, Acta Phys. Pol. A **104**, 123 (2003).
[19] J. Wu, W. Walukiewicz, W. Shan, K. M. Yu, J. W. Ager III, E. E. Haller, H. Lu, and W. J. Schaff, Phys. Rev. B **66**, 201403(R) (2002).
[20] R. Goldhahn, A. T. Winzer, V. Cimalla, O. Ambacher, C. Cobet, W. Richter, N. Esser, J. Furthmüller, F. Bechstedt, H. Lu, and W. J. Schaff, Superlattices Microstruct. **36**, 591 (2004).
[21] K. S. A. Butcher and T. L. Tansley, Superlattices Microstruct. **38**, 1 (2005).
[22] C. Persson, R. Ahuja, A. Ferreira da Silva, and B. Johansson, J. Phys.: Condens. Matter **13**, 8945 (2001).
[23] A. S. Barker and M. Ilegems, Phys. Rev. B **7**, 743 (1973).
[24] I. Vurgaftman and J. Meyer, J. Appl. Phys. **94**, 3675 (2003).
[25] E. O. Kane, J. Phys. Chem. Solids **1**, 249 (1957).
[26] S. Shokhovets, G. Gobsch, and O. Ambacher, Appl. Phys. Lett. **86**, 161908 (2005).
[27] T. D. Veal, L. F. J. Piper, M. R. Phillips, M. H. Zareie, H. Lu, W. J. Schaff, and C. F. McConville, Phys. Status Solidi A **203**, 85 (2006).
[28] I. Mahboob, T. D. Veal, L. F. J. Piper, C. F. McConville, H. Lu, W. J. Schaff, J. Furthmüller, and F. Bechstedt, Phys. Rev. B **69**, 201307(R) (2004).
[29] W. Walukiewicz, J. W. Ager III, K. M. Yu, Z. Liliental-Weber, J. Wu, S. X. Li, R. E. Jones, and J. D. Denlinger, J. Phys. D **39**, R83 (2006).
[30] S. Pereira, M. R. Correia, T. Monteiro, E. Pereira, E. Alves, A. D. Sequeira, and N. Franco, Appl. Phys. Lett. **78**, 2137 (2001).
[31] C. Wetzel, T. Takeuchi, S. Yamaguchi, H. Katoh, H. Amano, and I. Akasaki, Appl. Phys. Lett. **73**, 1994 (1998).
[32] K. Thonke, K. Kornitzer, M. Grehl, R. Sauer, C. Kirchner, V. Schwegler, M. Kamp, M. Leszczynski, I. Grzegory, and S. Porowski, in *Proceedings of the International Workshop on Nitride Semiconductors, Nagoya 2000, Conference Series 1* (The Institute of Pure and Applied Physics, Tokyo, 2001), p. 587.
[33] Z. Dridi, B. Bouhafs, and P. Ruterana, Semicond. Sci. Technol. **18**, 850 (2003).
[34] C. Caetano, L. K. Teles, M. Marques, A. Dal Pino Jr., and L. G. Ferreira, Phys. Rev. B **74**, 045215 (2006).
[35] J. Furthmüller, P. H. Hahn, F. Fuchs, and F. Bechstedt, Phys. Rev. B **72**, 205106 (2005).
[36] M. Losurdo, G. Bruna, T.-H. Kim, S. Choi, and A. Brown, Appl. Phys. Lett. **88**, 121928 (2006).
[37] M. Drago, P. Vogt, and W. Richter, Phys. Status Solidi A **203**, 116 (2006).
[38] D. E. Aspnes, Phys. Rev. Lett. **28**, 168 (1972).
[39] C. Buchheim, R. Goldhahn, M. Rakel, C. Cobet, N. Esser, U. Rossow, D. Fuhrmann, and A. Hangleiter, Phys. Status Solidi B **242**, 2610 (2005).
[40] R. Goldhahn, C. Buchheim, P. Schley, A. T. Winzer, and H. Wenzel, in *Nitride Semiconductor Devices: Principles and Simulation*, edited by J. Piprek (Wiley, Weinheim, 2007), p. 95.